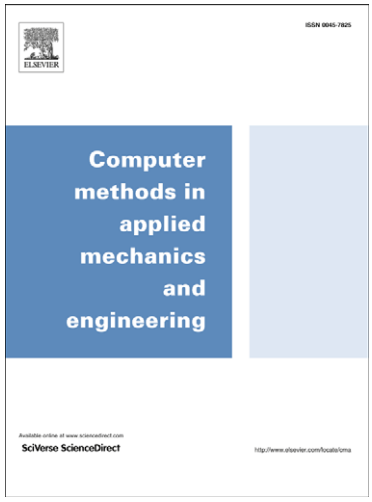

An Unconditionally Energy-stable Method for the Phase Field Crystal Equation

Hector Gomez, Xesús Nogueira

PII: S0045-7825(12)00069-2
DOI: 10.1016/j.cma.2012.03.002
Reference: CMA 9664

To appear in: *Comput. Methods Appl. Mech. Engrg.*

Received Date: 22 October 2011
Revised Date: 1 March 2012
Accepted Date: 2 March 2012

Please cite this article as: H. Gomez, X. Nogueira, An Unconditionally Energy-stable Method for the Phase Field Crystal Equation, *Comput. Methods Appl. Mech. Engrg.* (2012), doi: 10.1016/j.cma.2012.03.002

An Unconditionally Energy-stable Method for the Phase Field Crystal Equation

Hector Gomez[1] * , Xesús Nogueira[1]

1: Group of Numerical Methods in Engineering
University of A Coruña
Department of Mathematical Methods
Campus de Elviña, s/n
15192, A Coruña

Abstract

The phase field crystal equation has been recently put forward as a model for microstructure evolution of two-phase systems on atomic length and diffusive time scales. The theory is cast in terms of an evolutive nonlinear sixth-order partial differential equation for the interatomic density that locally minimizes an energy functional with the constraint of mass conservation. Here we propose a new numerical algorithm for the phase field crystal equation that is second-order time-accurate and unconditionally stable with respect to the energy functional. We present several numerical examples in two and three dimensions dealing with crystal growth in a supercooled liquid and crack propagation in a ductile material. These examples show the effectiveness of our new algorithm.

Key words: Isogeometric Analysis, Time-integration, Unconditionally stable, Phase-field crystal

1 Introduction

Material properties at the meso- and macro-scales are to a large extent controlled by complex microstructures exhibiting topological defects, such as, for example, vacancies, grain boundaries and dislocations. These defects are the result of complicated non-equilibrium dynamics that takes place on atomic length scales. The modeling and simulation of the

* Correspondence to: University of A Coruña, Deparment of Mathematical Methods
Email address: hgomez@udc.es (Hector Gomez[1]).

onset and evolution of these features poses significant challenges over current multiscale techniques. Typically, predictive models for these phenomena take the form of Molecular Dynamics simulations, which describe them with significant accuracy, but are limited by atomic length scales and femtosecond time scales. Continuum theories permit simulating much larger systems and longer times, but usually fall short of incorporating the fundamental physical features that govern microstructure evolution. Recently, a new theory has been put forward under the name of phase field crystal equation [17,18,42]. This model describes the microstructure of two-phase systems on atomic length scales, but on a diffusive time scale, leading to significant computational savings compared to Molecular Dynamics simulations. The phase field crystal equation has been employed to simulate a number of physical phenomena, including crystal growth in a supercooled liquid, dendritic and eutectic solidification, epitaxial growth, and crack propagation in a ductile material [17,42]. The phase field crystal equation is derived from an energy functional that is minimized by periodic density fields, naturally incorporating the periodicity of a crystal lattice. The model is then cast as an evolutive sixth-order partial differential equation (PDE) that locally minimizes this energy functional under the constraint of mass conservation.

The numerical simulation of the phase field crystal equation presents several challenges, such as, for example, the discretization of nonlinear higher-order partial-differential operators and the approximation of dynamic interfaces that travel over the computational domain. Previous work on the topic include [11,32–34,49,54]. Given the fact that the exact solutions to the phase field crystal equation lead to a time-decreasing energy functional, we feel that a significant goal in the numerical simulation of this model is the development of algorithms that verify this property at the discrete level irrespectively of the coarseness of the discretization (in what follows, algorithms of this type will be called unconditionally energy stable or thermodynamically consistent). Thermodynamically consistent methods have been previously studied in the context of solid [3,39,44,45] and fluid mechanics [30,36,47,48], but remain less investigated for phase-field equations (significant works on this topic include [16,20,22,24,27,31,51–53]). Remarkably, a second-order accurate, unconditionally uniquely solvable algorithm for the phase field crystal equation has been proposed in [34,54]. This scheme is unconditionally stable with respect to a discrete energy and weakly stable with respect to the physical energy. Here we introduce a new fully-discrete algorithm for the phase field crystal equation that is second-order time accurate and unconditionally energy stable. Our time integration algorithm is based on a new quadrature formula proposed in [27] that may be thought of as a non-symmetric higher-order extension of the trapezoidal rule. Our space discretization is based on a new mixed variational form of the phase field crystal equation. The well-posedness of our variational form requires the use of globally $\mathcal{C}^1$-continuous basis functions that we generate using Isogeometric Analysis [12,35], a recently proposed generalization of Finite Element Analysis.

We present several numerical examples in two and three dimensions dealing with crystal growth in a supercooled liquid, and crack propagation in a ductile material. These examples show the effectiveness of our approach. The outline of this paper is as follows: In section 2, we describe the phase field crystal equation. Section 3 presents our algorithm for this equation. We present numerical examples in section 4. Finally, we draw conclusions in section 5.

2 The phase field crystal equation

The phase field crystal equation describes the microstructure of solid-liquid systems at interatomic length scales, and at a diffusive time scale [17,18]. The two-phase system is described by a local atomistic density field ρ, which will be approximately uniform in the liquid phase, and will inherit the symmetry and periodicity of the crystal lattice in the solid phase. The phase field crystal equation has been shown to correctly model the dynamics of crystal growth, including naturally elastic and plastic deformations. Other physical phenomena for which the phase field crystal equation has shown potential as a predictive tool include epitaxial growth, material hardness, grain growth, reconstructive phase transitions, and crack propagation in ductile materials [17]. The phase field crystal equation has also been recently employed to model foams [29] and colloidal solidification [50].

The fundamental quantity for the phase field crystal equation is the following Lyapunov functional:

$$\mathcal{F}(\rho) = \int_\Omega \left\{ \Phi(\rho) + \frac{D}{2}\left[(\Delta\rho)^2 - 2k^2|\nabla\rho|^2 + k^4\rho^2 \right] \right\} \mathrm{d}\boldsymbol{x} \tag{1}$$

where k and D are positive numbers, and

$$\Phi(\rho) = -\frac{\epsilon}{2}\rho^2 - \frac{g}{3}\rho^3 + \frac{1}{4}\rho^4 \tag{2}$$

In equation (2), ϵ and g are positive constants with physical significance. The phase field crystal equation was derived as an evolutive PDE that preserves mass throughout the entire dynamical process, and achieves free-energy dissipation. These requirements lead us to the equation

$$\frac{\partial\rho}{\partial t} = \Delta\left(\frac{\delta\mathcal{F}}{\delta\rho}\right) \tag{3}$$

where $\delta\mathcal{F}/\delta\rho$ denotes the variational derivative of $\mathcal{F}$ with respect to ρ. Note that equation (3) follows the typical structure of conserved phase-field models [2,7–10,14,15,21], and satisfies the aforementioned properties. Using the expression of the variational derivative of $\mathcal{F}$ and the notation $\varphi(\rho) = \Phi'(\rho)$, we get the phase field crystal equation

$$\frac{\partial\rho}{\partial t} = \Delta\left(\varphi(\rho) + Dk^4\rho + 2Dk^2\Delta\rho + D\Delta^2\rho\right) \tag{4}$$

which involves sixth-order partial derivatives in space.

Multiplying equation (3) with $\delta\mathcal{F}/\delta\rho$, integrating over the spatial domain Ω, and integrating by parts, the following expression may be obtained,

$$\frac{\mathrm{d}F}{\mathrm{d}t} = -\int_\Omega \left| \nabla\left(\frac{\delta\mathcal{F}}{\delta\rho}\right) \right|^2 \mathrm{d}\boldsymbol{x} \tag{5}$$

where F is a real-valued function defined as $F(t) = \mathcal{F}(\rho(\cdot,t))$. Equation (5) shows that the energy functional (1) decreases in time over fields ρ which satisfy the phase field crystal equation.

2.1 Initial/boundary-value problem

We state the following initial/boundary-value problem over the spatial domain Ω and the time interval $(0,T)$: given $\rho_0 : \overline{\Omega} \mapsto \mathbb{R}$, find $\rho : \overline{\Omega} \times [0,T] \mapsto \mathbb{R}$ such that

$$\frac{\partial \rho}{\partial t} = \Delta\left(\varphi(\rho) + Dk^4\rho + 2Dk^2\Delta\rho + D\Delta^2\rho\right) \quad \text{in} \quad \Omega \times (0,T) \tag{6}$$

$$\nabla\left(\varphi(\rho) + Dk^4\rho + 2Dk^2\Delta\rho + D\Delta^2\rho\right)\cdot \boldsymbol{n} = 0 \quad \text{on} \quad \Gamma \times [0,T] \tag{7}$$

$$\nabla(2Dk^2\rho + D\Delta\rho)\cdot \boldsymbol{n} = 0 \quad \text{on} \quad \Gamma \times [0,T] \tag{8}$$

$$\nabla\rho \cdot \boldsymbol{n} = 0 \quad \text{on} \quad \Gamma \times [0,T] \tag{9}$$

$$\rho(\boldsymbol{x},0) = \rho_0(\boldsymbol{x}) \quad \text{in} \quad \overline{\Omega} \tag{10}$$

3 Numerical formulation for the phase-field crystal equation

Here we present our numerical formulation for the phase field crystal equation. We first derive a semidiscrete formulation, and then introduce a time integration scheme which preserves mass during the entire dynamical process, and is unconditionally energy stable.

3.1 Semidiscrete formulation

To derive the semidiscrete formulation we propose the following splitting of the phase field crystal equation,

$$\frac{\partial \rho}{\partial t} = \Delta\sigma \tag{11}$$

$$\sigma = \varphi(\rho) + Dk^4\rho + 2Dk^2\Delta\rho + D\Delta^2\rho \tag{12}$$

Let us define the functional space $\mathscr{V} \subset \mathcal{H}^2$, where $\mathcal{H}^2$ is the Sobolev space of square integrable functions with square integrable first and second derivatives. We derive a weak form of equations (11)–(12) by multiplying them with functions $w, q \in \mathscr{V}$, and integrating by parts. At this point, we assume periodic boundary conditions in all directions. The problem can be stated as: find $\rho, \sigma \in \mathscr{V}$ such that for all $w, q \in \mathscr{V}$

$$\left(w, \frac{\partial \rho}{\partial t}\right) + (\nabla w, \nabla\sigma) = 0 \tag{13}$$

$$(q,\sigma) - \left(q, \varphi(\rho) + Dk^4\rho\right) + \left(\nabla q, 2Dk^2\nabla\rho\right) - (\Delta q, D\Delta\rho) = 0 \tag{14}$$

We derive a semidiscrete formulation by replacing (13)–(14) by a finite-dimensional problem defined over the discrete space $\mathcal{V}^h \subset \mathcal{V}$. The problem can be stated as follows: find $\rho^h, \sigma^h \in \mathcal{V}^h$ such that for all $w^h, q^h \in \mathcal{V}^h$

$$\left(w^h, \frac{\partial \rho^h}{\partial t}\right) + \left(\nabla w^h, \nabla \sigma^h\right) = 0 \tag{15}$$

$$\left(q^h, \sigma^h\right) - \left(q^h, \varphi(\rho^h) + Dk^4\rho^h\right) + \left(\nabla q^h, 2Dk^2 \nabla \rho^h\right) - \left(\Delta q^h, D\Delta \rho^h\right) = 0 \tag{16}$$

Note that the condition $\mathcal{V}^h \subset \mathcal{V}$ requires the discrete space to be $\mathcal{H}^2$ conforming. We satisfy this requirement using Isogeometric Analysis [12,35], a recently proposed generalization of Finite Element Analysis. Isogeometric Analysis is based on developments of Computer Aided Design (CAD). The main idea of Isogeometric Analysis is to use the parametrizations that underlie CAD designs to generate the computational mesh and the basis functions necessary for analysis, following the isoparametric concept. This holds promise to simplify, or even eliminate altogether, the mesh generation and refinement process, currently the most time-consuming step of analysis. CAD parametrizations are usually defined in terms of Non-Uniform Rational B-Splines (NURBS), although there are other possibilities, such as, for example, T-Splines [4] or PHT-Splines [40]. NURBS are generated from B-Splines using projective transformations, while B-Splines are simply piecewise polynomials [41,43]. Thus, in NURBS-based Isogeometric Analysis, both the computational domain and the solution field are described using NURBS. This not only leads to simpler interface between CAD and analysis, but has also proven superior accuracy than classical Finite Elements on a per-degree-of-freedom basis [1,23]. Isogeometric Analysis has been successfully applied to a number of problems in solid [13,19,37,38] and fluid mechanics [5,6] showing significant efficiency and robustness. Even more importantly for the present work, the use of NURBS permits generating globally $\mathcal{C}^1$-continuous basis functions easily, which leads to a simple and efficient discretization of higher-order operators as shown in [25–28]. In what follows, we will suppose that $\mathcal{V}^h = \text{span}\{N_A\};\ A = 1, \ldots, n_b$, where N_A is a $\mathcal{C}^1$-continuous NURBS function associated to the global degree of freedom A and n_b is the dimension of the discrete space.

3.2 Time integration

This section presents our time integration scheme for the phase field crystal equation. We divide the time interval $[0, T]$ into subintervals $I_n = [t_n, t_{n+1}]$ where $0 = t_0 < t_1 < \cdots < t_N = T$ and $[0, T] = \cup_{n=0}^{N-1} I_n$. We define the time step $\Delta t_n = t_{n+1} - t_n$. Let us call ρ_n^h the time discrete approximation to $\rho^h(t_n)$. Thus, the problem can be stated as follows: given ρ_n^h, find $\rho_{n+1}^h \in \mathcal{V}^h$ such that for all $w^h, q^h \in \mathcal{V}^h$

$$\left(w^h, \frac{[\![\rho_n^h]\!]}{\Delta t_n}\right) + \left(\nabla w^h, \nabla \sigma^h\right) = 0 \tag{17}$$

$$\left(q^h, \sigma^h\right) - \left(q^h, \frac{1}{2}\left(\varphi(\rho_n^h) + \varphi(\rho_{n+1}^h)\right) - \frac{[\![\rho_n^h]\!]^2}{12}\varphi''(\rho_n^h)\right) - \left(q^h, Dk^4\rho_{n+1/2}^h\right)$$
$$+ \left(\nabla q^h, 2Dk^2\nabla\rho_{n+1/2}^h\right) - \left(\Delta q^h, D\Delta\rho_{n+1/2}^h\right) = 0 \tag{18}$$

where

$$[\![\rho_n^h]\!] = \rho_{n+1}^h - \rho_n^h \quad \text{and} \quad \rho_{n+1/2}^h = (\rho_{n+1}^h + \rho_n^h)/2 \tag{19}$$

We summarize in the following theorem the most relevant properties of our discrete formulation.

Theorem 1 *The fully-discrete variational formulation* (17)–(18)*:*

(1) Verifies mass conservation, that is,

$$\int_\Omega \rho_n^h \mathrm{d}\boldsymbol{x} = \int_\Omega \rho_0^h \mathrm{d}\boldsymbol{x} \quad \forall n = 1, \ldots, N$$

(2) Verifies the nonlinear stability condition

$$\mathcal{F}(\rho_n^h) \leq \mathcal{F}(\rho_{n-1}^h) \quad \forall n = 1, \ldots, N$$

irrespectively of the time step.

(3) Gives rise to a local truncation error τ that may be bounded as $|\tau(t_n)| \leq K\Delta t_n^2$ for all $t_n \in [0, T]$, where K is a constant independent of Δt_n.

Proof:

(1) The result can be proven taking $w^h = 1$ in equation (17), and applying inductive logic.

(2) The proof relies on the following quadrature formula: Let $f : [a, b] \mapsto \mathbb{R}$ be a sufficiently smooth function. It may be proven that

$$\int_a^b f(x)\mathrm{d}x = \frac{b-a}{2}\left(f(a) + f(b)\right) - \frac{(b-a)^3}{12}f''(a) - \frac{(b-a)^4}{24}f'''(\xi);\ \xi \in (a, b) \tag{20}$$

A complete derivation of this formula may be found in [27]. If we apply this quadrature formula to the right hand side of the identity

$$\int_{\rho_n^h}^{\rho_{n+1}^h} \Phi'(t)\mathrm{d}t = \int_{\rho_n^h}^{\rho_{n+1}^h} \varphi(t)\mathrm{d}t \tag{21}$$

we get

$$[\![\varphi(\rho_n^h)]\!] = \frac{[\![\rho_n^h]\!]}{2}\left(\varphi(\rho_n^h) + \varphi(\rho_{n+1}^h)\right) - \frac{[\![\rho_n^h]\!]^2}{12}\varphi''(\rho_n^h) - \frac{[\![\rho_n^h]\!]^4}{24}\varphi'''(\rho_{n+\epsilon}^h);\ \epsilon \in (0, 1) \tag{22}$$

Now, let us take $w^h = \sigma^h$ in (17) and $q^h = [\![\rho_n^h]\!]$ in (18). It follows that,

$$\left(\sigma^h, \frac{[\![\rho_n^h]\!]}{\Delta t_n}\right) + \left(\nabla\sigma^h, \nabla\sigma^h\right) = 0 \tag{23}$$

$$\left([\![\rho_n^h]\!], \sigma^h\right) - \left([\![\rho_n^h]\!], \frac{1}{2}\left(\varphi(\rho_n^h) + \varphi(\rho_{n+1}^h)\right) - \frac{[\![\rho_n^h]\!]^2}{12}\varphi''(\rho_n^h)\right) - \left([\![\rho_n^h]\!], Dk^4\rho_{n+1/2}^h\right)$$
$$+ \left(\nabla[\![\rho_n^h]\!], 2Dk^2\nabla\rho_{n+1/2}^h\right) - \left(\Delta[\![\rho_n^h]\!], D\Delta\rho_{n+1/2}^h\right) = 0 \tag{24}$$

Taking into account that,

$$([\![\rho_n^h]\!], \rho_{n+1/2}^h) = \frac{1}{2}\int_\Omega [\![(\rho_n^h)^2]\!]\mathrm{d}x;\ (\nabla[\![\rho_n^h]\!], \nabla\rho_{n+1/2}^h) = \frac{1}{2}\int_\Omega [\![|\nabla\rho_n^h|^2]\!]\mathrm{d}x; \tag{25}$$

$$(\Delta[\![\rho_n^h]\!], \Delta\rho_{n+1/2}^h) = \frac{1}{2}\int_\Omega [\![(\Delta\rho_n^h)^2]\!]\mathrm{d}x \tag{26}$$

and making use of (22), we conclude that

$$[\![\mathcal{F}(\rho_n^h)]\!] = -\Delta t_n\left(\nabla\sigma^h, \nabla\sigma^h\right) - \frac{1}{24}\left([\![\rho_n^h]\!]^4, \varphi'''(\rho_{n+\xi}^h)\right) \tag{27}$$

and the result is proven, because $\varphi'''(\rho) \geq 0\ \forall\rho \in \mathbb{R}$.

(3) We derive a bound on the local truncation error by comparing our method with the midpoint rule, which is known to be a second-order time-accurate algorithm. Applying the midpoint rule to the semidiscrete formulation of the phase field crystal equation (15)–(16), we obtain

$$\left(w^h, \frac{[\![\overline{\rho}_n^h]\!]}{\Delta t_n}\right) + \left(\nabla w^h, \nabla\overline{\sigma}^h\right) = 0 \tag{28}$$

$$\left(q^h, \overline{\sigma}^h - \varphi(\overline{\rho}_{n+1/2}^h) - Dk^4\overline{\rho}_{n+1/2}^h\right) + \left(\nabla q^h, 2Dk^2\nabla\overline{\rho}_{n+1/2}^h\right) - \left(\Delta q^h, D\Delta\overline{\rho}_{n+1/2}^h\right) = 0 \tag{29}$$

where equation (29) defines $\overline{\sigma}^h$, and $\overline{\rho}_{n+1}^h$ is the time discrete solution using the midpoint rule. The local truncation error of the midpoint rule may be obtained by replacing the time discrete solution $\overline{\rho}_n^h$ with the time continuous solution $\rho^h(t_n)$ in equations (28)–(29). The time continuous solution does not satisfy equations (28)–(29), giving rise to the local truncation error. Proceeding this way, we obtain

$$\left(w^h, \frac{[\![\rho^h(t_n)]\!]}{\Delta t_n}\right) + \left(\nabla w^h, \nabla\overline{\sigma}_\tau^h\right) = \left(w^h, \overline{\tau}(t_n)\right) \tag{30}$$

$$\left(q^h, \overline{\sigma}_\tau^h - \varphi\left(\rho^h(t_{n+1/2})\right) - Dk^4\rho^h(t_{n+1/2})\right) + \left(\nabla q^h, 2Dk^2\nabla\rho^h(t_{n+1/2})\right)$$
$$- \left(\Delta q^h, D\Delta\rho^h(t_{n+1/2})\right) = 0 \tag{31}$$

where $\overline{\sigma}_\tau^h$ is defined in equation (31), and $\overline{\tau}(t_n)$ is the local truncation error of the midpoint rule. Using Taylor series, it may be proven that $|\overline{\tau}(t_n)| \leq K\Delta t_n^2$, where K is a real constant independent of Δt_n. If we proceed analogously with our algorithm, we define the local truncation error of our method by replacing the time continuous solution in equations (17)–(18), which leads to

$$\left(w^h, \frac{[\![\rho^h(t_n)]\!]}{\Delta t_n}\right) + \left(\nabla w^h, \nabla \sigma_\tau^h\right) = \left(w^h, \tau(t_n)\right) \tag{32}$$

$$\left(q^h, \sigma_\tau^h - \frac{1}{2}\left(\varphi(\rho^h(t_n)) + \varphi(\rho^h(t_{n+1}))\right) - \frac{[\![\rho^h(t_n)]\!]^2}{12}\varphi''(\rho^h(t_n)) - Dk^4\rho^h(t_{n+1/2})\right)$$
$$+ \left(\nabla q^h, 2Dk^2\nabla\rho^h(t_{n+1/2})\right) - \left(\Delta q^h, D\Delta\rho^h(t_{n+1/2})\right) = 0 \tag{33}$$

Taking into account that

$$\frac{1}{2}\left(\varphi(\rho^h(t_n)) + \varphi(\rho^h(t_{n+1}))\right) - \frac{[\![\rho^h(t_n)]\!]^2}{12}\varphi''(\rho^h(t_n)) = \varphi(\rho^h(t_{n+1/2})) + \mathcal{O}(\Delta t_n^2) \tag{34}$$

it follows that,

$$\left(w^h, \overline{\tau}(t_n)\right) = \left(w^h, \tau(t_n)\right) + \mathcal{O}(\Delta t_n^2) \tag{35}$$

$$\left(q^h, \overline{\sigma}_\tau^h\right) = \left(q^h, \sigma_\tau^h\right) + \mathcal{O}(\Delta t_n^2) \tag{36}$$

which implies that there exists a real constant K, independent of Δt_n such that $|\tau(t_n)| \leq K\Delta t_n^2$, and the pursued result is proven.

□

3.3 Implementation

Let $\boldsymbol{P}_n$ and $\boldsymbol{S}_n$ be the global vectors of degrees of freedom associated to ρ_n^h and its corresponding σ^h, respectively. We introduce the following residual vectors

$$\boldsymbol{R}^\rho(\boldsymbol{P}_n, \boldsymbol{P}_{n+1}, \boldsymbol{S}_{n+1}); \quad \boldsymbol{R}^\rho = \{R_A^\rho\}; A = 1, \ldots, n_b \tag{37}$$

$$\boldsymbol{R}^\sigma(\boldsymbol{P}_n, \boldsymbol{P}_{n+1}, \boldsymbol{S}_{n+1}); \quad \boldsymbol{R}^\sigma = \{R_A^\sigma\}; A = 1, \ldots, n_b \tag{38}$$

where

$$R_A^\rho = \left(N_A, \frac{[\![\rho_n^h]\!]}{\Delta t}\right) + \left(\nabla N_A, \nabla \sigma^h\right) \tag{39}$$

$$R_A^\sigma = (N_A, \sigma^h) - \left(N_A, \frac{1}{2}\left(\varphi(\rho_{n+1}^h) + \varphi(\rho_n^h)\right) - \frac{[\![\rho_n^h]\!]^2}{12}\varphi''(\rho_n^h)\right)$$
$$- (N_A, Dk^4\rho_{n+1/2}^h) + \left(\nabla N_A, 2Dk^2\nabla\rho_{n+1/2}^h\right) - \left(\Delta N_A, D\Delta\rho_{n+1/2}^h\right) \tag{40}$$

When we equate these residual vectors to zero, we obtain a nonlinear system of equations for $\boldsymbol{P}_{n+1}$ and $\boldsymbol{S}_{n+1}$ that we solve using Newton's method.

Let $\boldsymbol{P}_{n+1,(i)}$ and $\boldsymbol{S}_{n+1,(i)}$ be the i-th iteration of Newton's algorithm. Our iterative procedure is defined as follows: Take $\boldsymbol{P}_{n+1,(0)} = \boldsymbol{P}_n$, and $\boldsymbol{S}_{n+1,(0)} = \boldsymbol{S}_n$. Then, for $i = 1, \ldots, i_{max}$

(1) Compute the residual vectors using the values $\boldsymbol{P}_{n+1,(i)}$, $\boldsymbol{S}_{n+1,(i)}$. These will be denoted as $\boldsymbol{R}^{\rho}_{(i)}$, $\boldsymbol{R}^{\sigma}_{(i)}$.
(2) Compute the tangent matrix $\boldsymbol{K}_{(i)}$ using the i-th iterates. This matrix has a block structure and may be written as

$$\boldsymbol{K}_{(i)} = \begin{pmatrix} \boldsymbol{K}^{\rho\rho}_{(i)} & \boldsymbol{K}^{\rho\sigma}_{(i)} \\ \boldsymbol{K}^{\sigma\rho}_{(i)} & \boldsymbol{K}^{\sigma\sigma}_{(i)} \end{pmatrix}$$

.
(3) Solve the linear system

$$\begin{pmatrix} \boldsymbol{K}^{\rho\rho}_{(i)} & \boldsymbol{K}^{\rho\sigma}_{(i)} \\ \boldsymbol{K}^{\sigma\rho}_{(i)} & \boldsymbol{K}^{\sigma\sigma}_{(i)} \end{pmatrix} \begin{pmatrix} \Delta\boldsymbol{P}_{(i+1)} \\ \Delta\boldsymbol{S}_{(i+1)} \end{pmatrix} = - \begin{pmatrix} \boldsymbol{R}^{\rho}_{(i)} \\ \boldsymbol{R}^{\sigma}_{(i)} \end{pmatrix}$$

using diagonally-preconditioned GMRES [46].
(4) Update the solution as,

$$\begin{pmatrix} \boldsymbol{P}_{n+1,(i+1)} \\ \boldsymbol{S}_{n+1,(i+1)} \end{pmatrix} = \begin{pmatrix} \boldsymbol{P}_{n+1,(i)} \\ \boldsymbol{S}_{n+1,(i)} \end{pmatrix} + \begin{pmatrix} \Delta\boldsymbol{P}_{(i+1)} \\ \Delta\boldsymbol{S}_{(i+1)} \end{pmatrix}$$

The process (1)-(4) needs to be repeated until the norms of both residual vectors have been reduced to a given tolerance *tol* of their initial value. Taking $tol = 10^{-4}$, convergence is typically achieved in two or three iterations.

Remark:

An important topic that is, however, out of the scope of this paper is the solvability of the nonlinear system of equations (37)–(40). In principle, the unique solvability of this nonlinear system of equations may impose a restriction on the time step size. Our numerical simulations indicate that this potential restriction, if existed, would be very mild, because for all the numerical examples that we performed, we have been able to take time steps larger than those reported in the literature. We also remark that the algorithm proposed by Hu et al. [34] is second-order accurate and unconditionally uniquely solvable. The trade-off for the sake of unconditional solvability is that Hu's method is not unconditionally stable with respect to the physical energy, but with respect to a slightly modified energy.

4 Numerical examples

In this section we present some numerical examples for the phase field crystal equation. The examples are related to several physical phenomena, such as, for instance, the growth of a polycrystal in a supercooled liquid, and the dynamic propagation of a crack in a ductile

material. Our calculations provide numerical corroboration for the theoretical results presented in the previous sections, and illustrate the accuracy, stability and robustness of our new algorithm.

4.1 Crystal growth in a supercooled liquid in two dimensions

This example presents the growth of a polycrystal in a supercooled liquid. We simulate the evolution of three crystallites with different orientations. This leads to a complex dynamical process which simultaneously involves the motion of liquid-crystal interfaces and grain boundaries separating the crystals. Similar numerical examples may be found in [18,34].

To define the initial configuration we proceed as follows: first; we set all control variables to a constant value $\bar{\rho}$, which for this example takes the value $\bar{\rho} = 0.285$; second; we modify this constant configuration by setting three perfect crystallites in three small square patches of the domain as illustrated in Figure 6(a). We use the following expression to define the crystallites:

$$\rho(x_l, y_l) = \bar{\rho} + C\left[\cos\left(\frac{q}{\sqrt{3}}y_l\right)\cos\left(qx_l\right) - 0.5\cos\left(\frac{2q}{\sqrt{3}}y_l\right)\right] \tag{41}$$

where x_l and y_l define a local system of cartesian coordinates that is oriented with the crystallite lattice. The parameters C and q take the values $C = 0.446$, and $q = 0.66$. To generate crystallites with different orientations, we define the local coordinates (x_l, y_l) using an affine transformation of the global coordinates (x, y), that produces a rotation given by an angle α. We generated the three crystallites using this strategy. We took $\alpha = -\pi/4$, $\alpha = 0$ and $\alpha = \pi/4$. Figure 6(a), which is the computed solution at an early time, gives a precise idea of the initial condition we employed.

The computational domain for this example is $\overline{\Omega} = [0, 800]^2$. On this domain, we define an uniform computational mesh composed of 2048^2 $\mathcal{C}^1$ quadratic elements. The time step is $\Delta t = 4$. The parameters of the phase field crystal equation take the values $D = k = 1$, $g = 0$, and $\epsilon = 0.25$.

Figure 6 shows snapshots of the numerical solution at several computational times. We observe the growth of the crystalline phase and the motion of well-defined crystal-liquid interfaces. The different alignment of the crystallites causes defects and dislocations that are clearly observed in the pictures. The solution presents similar features to those obtained in [18,34].

Figure 6 analyzes the time evolution of the energy functional. We recomputed this example using three different time steps, namely, $\Delta t = 1$, $\Delta t = 2$, $\Delta t = 4$, and plotted the free-energy evolution. The plot shows that the free energy is time decreasing in all cases, and the differences between the three cases are negligible. The inset in Figure 6 is a zoom of the energy evolution in the late dynamics of the equation. The inset shows that the larger is the time step, the higher is the energy at a given time, which is consistent with our previous experience with unconditionally stable methods for phase dynamics [27]. Additional insight

about the dependence of the energy evolution on the time step may be obtained examining equation (27).

4.2 Crack propagation on a square domain

Following [17], we utilize the phase field crystal equation to model crack propagation in a ductile material. We consider a square domain $\overline{\Omega} = [0, 1024\pi/3]^2$. The computational mesh is composed of 1024^2 $\mathcal{C}^1$ quadratic elements, and the time step is $\Delta t = 20$. We assume periodic boundary conditions in both directions. The parameters of the phase field crystal equation are $D = k = \epsilon = 1$, and $g = 0$. As initial condition, we set a crystal lattice given by the expression

$$\rho_0(\boldsymbol{x}) = 0.49 + \cos(q_x x)\cos\left(\frac{q_y}{\sqrt{3}}y\right) - \frac{1}{2}\cos\left(\frac{2q_y}{\sqrt{3}}y\right) \tag{42}$$

A crystal under no mechanical loads would be in equilibrium when $q_x = q_y = \sqrt{3}/2$ in the limit $\epsilon \to 0$. We take $q_x = 0.7265625000000$, and $q_y = 0.7307089344312$, which induces stretchings with respect to the equilibrium wavelength of approximately 16% and 15% in the x and y directions, respectively. These values of q_x and q_y also ensure that the initial condition is periodic, and, thus, compatible with boundary conditions. In the center of the domain, we set a small notch in which the density takes an homogeneous value of 0.79. We performed simulations using circular and square notches. The numerical approximation to the atomistic density field may be observed in Figure 3. We notice that the solution is extremely dependent on the shape of the notch. This is not surprising due to the high nonlinearity of the phase field crystal equation and the fact that different notch shapes induce different stress concentrations.

Figure 4 shows the time evolution of the energy functional for the two computations presented in Figure 3. We observe that the energy is decreasing at all times.

4.3 Crack propagation on a rectangular domain

For this calculation we consider the rectangular domain $\overline{\Omega} = [0, 2048\pi/3] \times [0, 512\pi/3]$. The computational mesh is composed of 2048×512 $\mathcal{C}^1$ quadratic elements. We assume periodic boundary conditions in both directions. The parameters of the phase field crystal equation are $D = k = \epsilon = 1$, and $g = 0$. The time step is $\Delta t = 20$. We remark that similar calculations presented in [17] employed a time step 400 times smaller, which indicates that our method is significantly more effective.

The initial condition is generated using formula (42), but we take different stretchings than in the last example. We perform two computations that correspond to two different mechanical configurations.

Configuration 1

We define configuration 1 taking $q_x = 0.8525390625000$, and $q_y = 0.7713038752455$ which induces stretchings of approximately 1% and 11% in the x and y directions, respectively. In this initial density field, we define a rectangular notch in which the density takes the constant value 0.79. The initial condition may be observed in Figure 5(a). As the computation evolves, the crack propagates over a straight horizontal line, leading to the situation depicted in Figure 5(b).

Configuration 2

Configuration 2 is defined taking $q_x = 0.7705078125000$, and $q_y = 0.7713038752455$ which induces stretchings of approximately 11% in both directions. For this example, we set two rectangular notches in which the density takes the value 0.79. The initial condition may be observed in Figure 6(a). This configuration leads to more complicated cracks that interact with each other. The numerical solution at time $t = 24000$ may be observed in Figure 6(b).

Figure 7 shows the time evolution of the free energy for the two mechanical configurations. It is observed that the energy decreases at all times.

4.4 Crystal growth in a supercooled liquid in three dimensions

This example deals with the numerical simulation of crystal growth in three dimensions. We simulate the growth and interaction of two crystallites that originate from two nucleation sites. The computational domain is $\overline{\Omega} = [0, 100]^3$, and we assume periodic boundary conditions in all directions. The parameters of the phase field crystal equation are $D = k = \epsilon = 1$ and $g = 0$. For this calculation, we employed an uniform mesh composed of 128^3 $\mathcal{C}^1$-quadratic elements. We utilized the time step $\Delta t = 1$. The initial configuration, depicted in Figure 8(a)-(b) was generated as follows: we let a randomly perturbed constant (liquid) state evolve to a periodic lattice (solid) state using the set up and parameters mentioned above. We extracted two pieces of the final state with an hexahedric shape, and superposed them to a constant density field as shown in Figure 8(a)-(b). In Figure 8, snapshot (a) shows isosurfaces of the density field, while image (b) presents a slice of the solution across the indicated plane. The evolution of the two crystallites may be observed in the second and third rows of Figure 8 (again, the left hand side shows isosurfaces, while the right hand side presents a slice of the solution across a plane). At some point the crystallites have grown enough as to start interacting as shown in Figure 9.

The asymptotic state, which can be observed in the third row of Figure 9 (snapshots (e)-(f)), corresponds to a solid state represented by a periodic lattice.

Figure 10 shows the time history of the energy functional (1). It may be observed that the energy decreases at all times, which, again, provides numerical evidence for our method being unconditionally stable.

5 Conclusions

The phase field crystal equation is a higher-order nonlinear PDE endowed with an stability property. It describes the microstructure of two-phase systems at interatomic length scales. We introduce new space-time discretizations that inherit the nonlinear stability relationship of the continuous equation irrespectively of the mesh and time step sizes, and that are second-order time-accurate. We utilize our new algorithm to compute a number of numerical examples that deal with several physical phenomena, such as, for example, crystal growth, and dynamic crack propagation. These examples provide numerical corroboration for our theoretical results, and show the accuracy, efficiency and robustness of our new method.

6 Acknowledgements

The authors were partially supported by *Xunta de Galicia* (grants # 09REM005118PR and #09MDS00718PR), *Ministerio de Ciencia e Innovacion* (grant #DPI2009-14546-C02-01) cofinanced with FEDER funds, and *Universidad de A Coruña*.

References

[1] I. Akkerman, Y. Bazilevs, V. M. Calo, T. J. R. Hughes, S. Hulshoff, The role of continuity in residual-based variational multiscale modeling of turbulence, *Computational Mechanics* **41** (2007) 371–378.

[2] D.M. Anderson, G.B. McFadden, A.A. Wheeler, Diffuse-interface methods in fluid mechanics, *Annu. Rev. Fluid Mech.* **30** (1998) 139–165.

[3] F. Armero, C. Zambrana-Rojas, Volume-preserving energy-momentum schemes for isochoric multiplicative plasticity, *Computer Methods in Applied Mechanics and Engineering* **196** (2007) 4130-4159.

[4] Y. Bazilevs, V.M. Calo, J.A. Cottrell, J.A. Evans, T.J.R. Hughes, S. Lipton, M.A. Scott, T.W. Sederberg, Isogeometric Analysis using T-splines, *Computer Methods in Applied Mechanics and Engineering*, **199** (2010) 229–263.

[5] Y. Bazilevs, V.M. Calo, J.A. Cottrell, T.J.R. Hughes, A. Reali, G. Scovazzi, Variational multiscale residual-based turbulence modeling for large eddy simulation of incompressible flows, *Computer Methods in Applied Mechanics and Engineering* **197** (2007) 173–201.

[6] Y. Bazilevs, T.J.R. Hughes, NURBS-based isogeometric analysis for the computation of flows about rotating components, *Computational Mechanics* **43** (2008) 143–150.

[7] J. Becker, G. Grün, R. Seemann, H. Mantz, K. Jacobs, K.R. Mecke, R. Blossey, Complex dewetting scenarios captured by thin-film models, *Nature Materials* **2** (2003) 59–63.

[8] J.W. Cahn, J.E. Hilliard, Free energy of a non-uniform system. I. Interfacial free energy, *The Journal of Chemical Physics* **28** (1958) 258–267.

[9] J.W. Cahn, J.E. Hilliard, Free energy of a non-uniform system. III. Nucleation in a two-component incompressible fluid, *The Journal of Chemical Physics* **31** (1959) 688–699.

[10] L.Q. Chen, Phase-field models for microstructural evolution, *Ann. Rev. Mater. Res.* **32** (2002) 113–140.

[11] M. Cheng, J.A. Warren, An efficient algorithm for solving the phase-field crystal model, *Journal of Computational Physics*, **227**, 6241–6248, 2008.

[12] J.A. Cottrell, T.J.R. Hughes, Y. Bazilevs, Isogeometric Analysis: Toward integration of CAD and FEA, John Wiley & Sons, Chichester, 2009.

[13] J.A. Cottrell, T.J.R. Hughes, A. Reali, Studies of refinement and continuity in isogeometric structural analysis, *Computer Methods in Applied Mechanics and Engineering*, **196** (2007) 4160–4183.

[14] L. Cueto-Felgueroso, R. Juanes, Nonlocal interface dynamics and pattern formation in gravity-driven unsaturated flow through porous media, *Physical Review Letters* **101** (2008) 244504.

[15] L. Cueto-Felgueroso, R. Juanes, A phase-field model of unsaturated flow, *Water Resources Research*, **45** W10409, (2009).

[16] Q. Du, R.A. Nicolaides, Numerical analysis of a continuum model of phase transition, *SIAM Journal of Numerical Analysis* **28** (1991) 1310–1322.

[17] K.R. Elder, M. Grant, Modeling elastic and plastic deformations in nonequilibrium processing using phase field crystals, *Physical Review E* **70** (2004) 051605.

[18] K.R. Elder, M. Katakowski, M. Haataja, M. Grant, Modeling elasticity in crystal growth, *Physical Review Letters* **88** (2002) 245701.

[19] T. Elguedj, Y. Bazilevs, V.M. Calo, T.J.R. Hughes, $\bar{B}$ and $\bar{F}$ projection methods for nearly incompressible linear and non-linear elasticity and plasticity using higher-order NURBS elements, *Computer Methods in Applied Mechanics and Engineering* **197** (2008) 2732–2762.

[20] C. Elliot, The Cahn-Hilliard model for the kinetics of phase separation, in *Mathematical Models for Phase Change Problems*, J.F. Rodrigues Ed., 1989.

[21] H. Emmerich, *The diffuse interface approach in materials science*, Springer, 2003.

[22] D.J. Eyre, An unconditionally stable one-step scheme for gradient systems, unpublished, www.math.utah.edu/∼eyre/research/methods/stable.ps

[23] J.A. Evans, Y. Bazilevs, I. Babuška, T.J.R. Hughes, n-widths, sup infs, and optimality ratios for the k-version of the isogeometric finite element method, *Computer Methods in Applied Mechanics and Engineering*, **198** (2009) 1726–1741.

[24] D. Furihata, A stable and conservative finite difference scheme for the Cahn-Hilliard equation, *Numer. Math.* **87** (2001) 675–699.

[25] H. Gomez, V.M. Calo, Y. Bazilevs, T.J.R. Hughes, Isogeometric analysis of the Cahn-Hilliard phase-field model, *Computer Methods in Applied Mechanics and Engineering* **197** (2008) 4333–4352.

[26] H. Gomez, T.J.R. Hughes, X. Nogueira, V.M. Calo, Isogeometric analysis of the isothermal Navier-Stokes-Korteweg equations, *Computer Methods in Applied Mechanics and Engineering* **199** 1828–1840.

[27] H. Gomez, T.J.R. Hughes, Provably unconditionally stable, second-order time-accurate, mixed variational methods for phase-field models, *Journal of Computational Physics*, **230**, 5310–5327, 2011.

[28] H. Gomez, J. París, Numerical simulation of asymptotic states of the damped Kuramoto-Sivashinsky equation, *Physical Review E*, **83**, 046702, 2011.

[29] N. Guttenberg, N. Goldenfeld, J. Dantzig, Emergence of foams from the breakdown of the phase field crystal model, *Physical Review E*, **81**, 065301(R), 2010.

[30] A. Harten, On the symmetric form of systems of conservation laws with entropy, *Journal of Computational Physics* **49** (1983) 151–164.

[31] L. He, Y. Liu, A class of stable spectral methods for the Cahn-Hilliard equation, *Journal of Computational Physics* **228** (2009) 5101–5110.

[32] T. Hirouchi, T. Takaki, Y. Tomita, Development of numerical scheme for phase field crystal deformation simulation, *Computational Material Science* **44** 1192–1197, 2009.

[33] T. Hirouchi, T. Takaki, Y. Tomita, Effects of temperature and grain size on phase-field-crystal deformation simulation, *International Journal of Mechanical Sciences* **52** 309–319, 2010.

[34] Z. Hu, S.M. Wise, C. Wang, J.S. Lowengrub, Stable and efficient finite-difference nonlinear multigrid schemes for the phase field crystal equation, *Journal of Computational Physics* **228** (2009) 5323–5339.

[35] T.J.R. Hughes, J.A. Cottrell, Y. Bazilevs, Isogeometric analysis: CAD, finite elements, NURBS, exact geometry and mesh refinement, *Computer Methods in Applied Mechanics and Engineering*, **194** (2005) 4135–4195.

[36] T.J.R. Hughes, L.P. Franca, M. Mallet, A new finite element formulation for computational fluid dynamics: I. Symmetric forms of the compressible Euler and Navier-Stokes equations and the second law of thermodynamics, *Computer Methods in Applied Mechanics and Engineering*, **54** (1986) 223–234.

[37] T.J.R Hughes, A. Reali, G. Sangalli, Duality and unified analysis of discrete approximations in structural dynamics and wave propagation: comparison of p-method finite elements with k-method NURBS, *Computer Methods in Applied Mechanics and Engineering* **197** (2008) 4104–4124.

[38] S. Lipton, J.A. Evans, Y. Bazilevs, T. Elguedj, T.J.R. Hughes, Robustness of isogeometric structural discretizations under severe mesh distortion, *Computer Methods in Applied Mechanics and Engineering*, **199** (2010) 357–373.

[39] X.N. Meng and T.A. Laursen, Energy consistent algorithms for dynamic finite deformation plasticity, *Computer Methods in Applied Mechanics and Engineering* **191** (2002) 1639–1675.

[40] N. Nguyen-Thanh, H. Nguyen-Xuan, S.P.A. Bordas, T. Rabczuk, Isogeometric analysis using polynomial splines over hierarchical T-meshes for two-dimensional elastic solids, *Computer Methods in Applied Mechanics and Engineering*, **200**, 1892–1908, 2011.

[41] L. Piegl, W. Tiller, *The NURBS Book*, Springer-Verlag, New York, 1997.

[42] N. Provatas, J.A. Dantzig, B. Athreya, P. Chan, P. Stefanovic, N. Goldenfeld, K.R. Elder, Using the phase-field crystal method in the multi-scale modeling of microstructure evolution, *Journal of the Minerals, Metals and Materials Society* **59**(7), 83–90, 2007.

[43] D.F. Rogers, *An introduction to NURBS: with historical perspective*, Morgan Kaufmann, 2001

[44] I. Romero, Algorithms for coupled problems that preserve symmetries and the laws of thermodynamics: Part I: Monolithic integrators and their application to finite strain thermoelasticity, *Computer Methods in Applied Mechanics and Engineering*, **199** (2010) 1841–1858.

[45] I. Romero, Algorithms for coupled problems that preserve symmetries and the laws of thermodynamics: Part II: Fractional step methods, *Computer Methods in Applied Mechanics and Engineering*, **199** (2010) 2235–2248.

[46] Y. Saad, M.H. Schultz, GMRES: A generalized minimal residual algorithm for solving nonsymmetric linear systems, *SIAM Journal of Scientific and Statistical Computing* **7** (1986) 856–869.

[47] F. Shakib, T.J.R. Hughes, Z. Johan, A new finite element formulation for computational fluid-dynamics. 10. The compressible Euler and Navier-Stokes equations, *Computer Methods in Applied Mechanics and Engineering* **89** (1991) 141–219.

[48] E. Tadmor, Skew-selfadjoint form for systems of conservation laws, *Journal of Mathematical Analysis and Applications* **103** (1984) 428–442.

[49] G. Tegze, G. Bansel, G.I. Tóth, T. Pusztai, Advanced operator splitting-based semi-implicit spectral method to solve the binary phase-field crystal equations with variable coefficients, *Journal of Computational Physics*, **228** 1612–1623, 2009.

[50] S. van Teeffelen, R. Backofen, A. Voigt, H. Löwen, Derivation of the phase-field-crystal model for colloidal solidification, *Physical Review E*, **79**, 051404, 2009.

[51] C. Wang, X. Wang, S.M. Wise, Unconditionally stable schemes for equations of thin film epitaxy, *Discrete Continuous and Dynamical Systems*, Series A, **28** 405–423, 2010.

[52] C. Wang, S.M. Wise, An energy stable and convergent finite difference scheme for the modified phase field crystal equation, *SIAM Journal Numerical Analysis*, **49** 945–969, 2011.

[53] S.M. Wise, Unconditionally stable finite difference, nonlinear multigrid simulation of the Cahn-Hilliard-Hele-Shaw system of equations, *Journal Scientific Computing*, **44** 38–68, 2010.

[54] S.M. Wise, C. Wang, J.S. Lowengrub, An energy-stable and convergent finite-difference scheme for the phase field crystal equation, *SIAM Journal of Numerical Analysis*, **47**(3), 2269–2288, 2009.

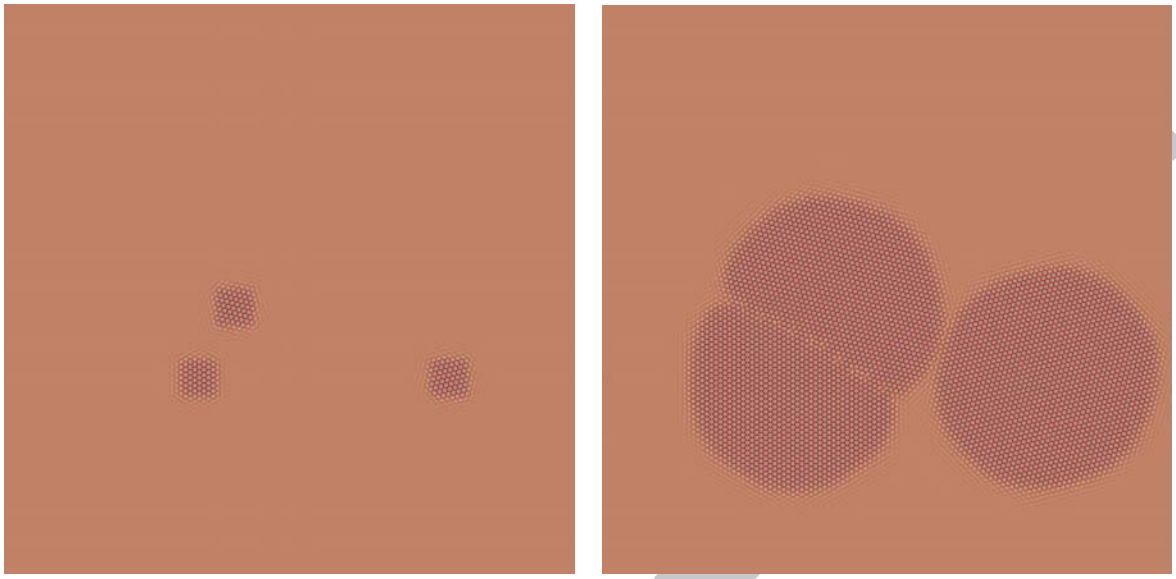

(a) $t = 20$ (b) $t = 400$

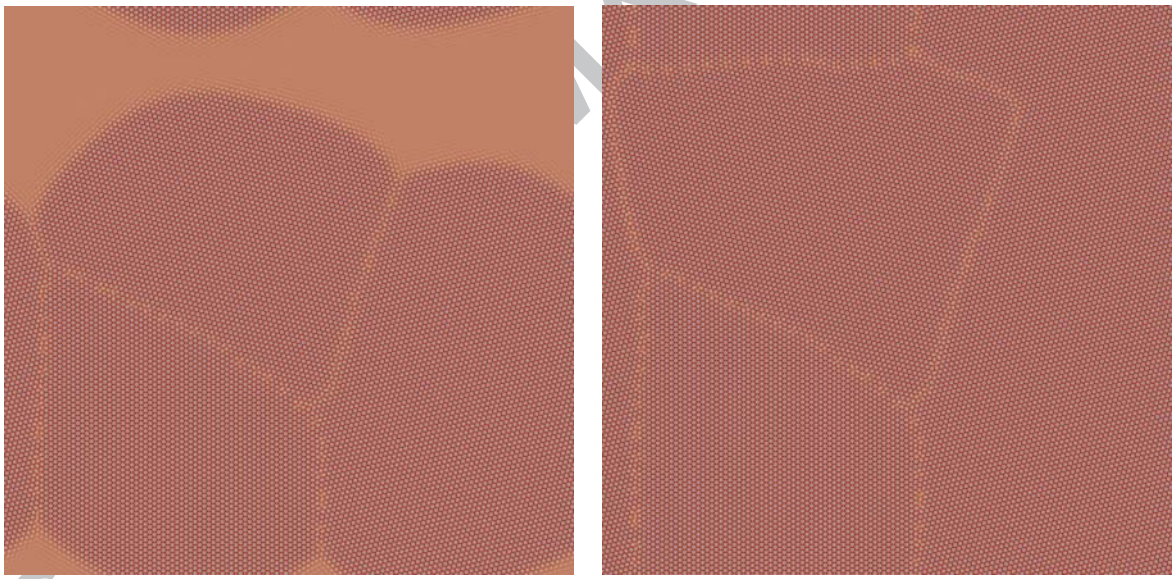

(c) $t = 800$ (d) $t = 1300$

Fig. 1. Crystal growth in a supercooled liquid. Snapshots of the numerical approximation to the atomistic density field. The parameters of the phase field crystal equation are $D = k = 1$, $g = 0$, and $\epsilon = 0.25$. The computational mesh is composed of 2048^2 $\mathcal{C}^1$ quadratic elements. The time step is $\Delta t = 4$.

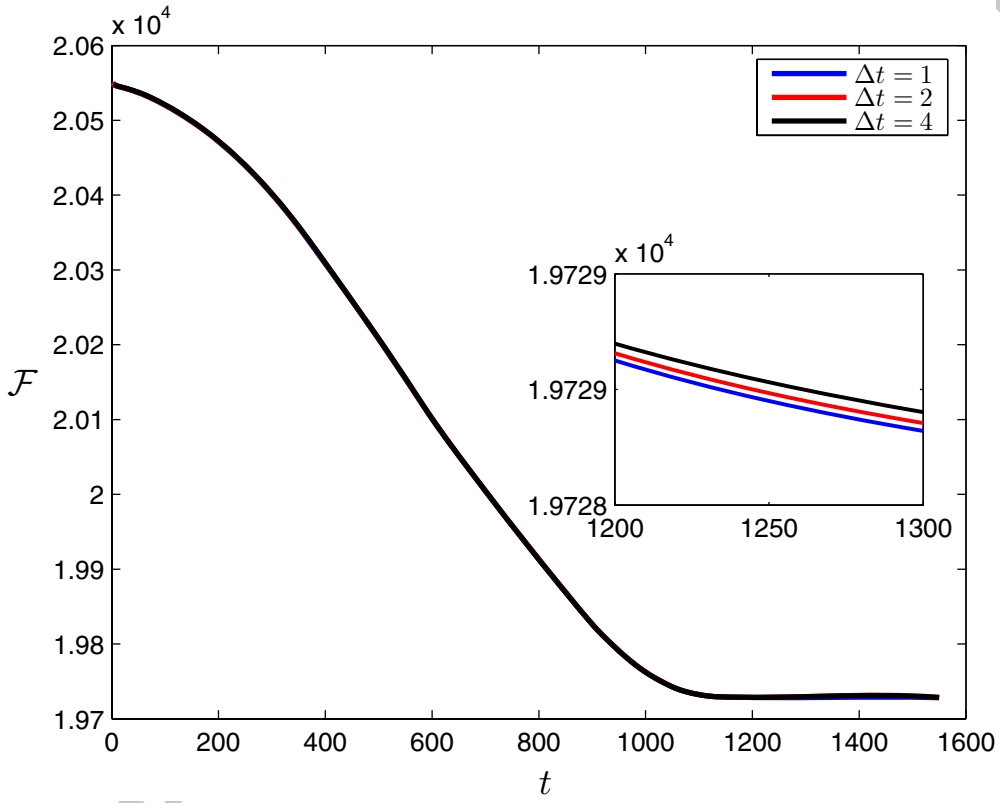

Fig. 2. Crystal growth in a supercooled liquid. Time evolution of the free energy functional for three different time steps. We observe that the energy decreases at all times, which confirms that our algorithm is unconditionally stable, as predicted by the theory. The inset shows the small differences in the energy evolution for the considered time steps.

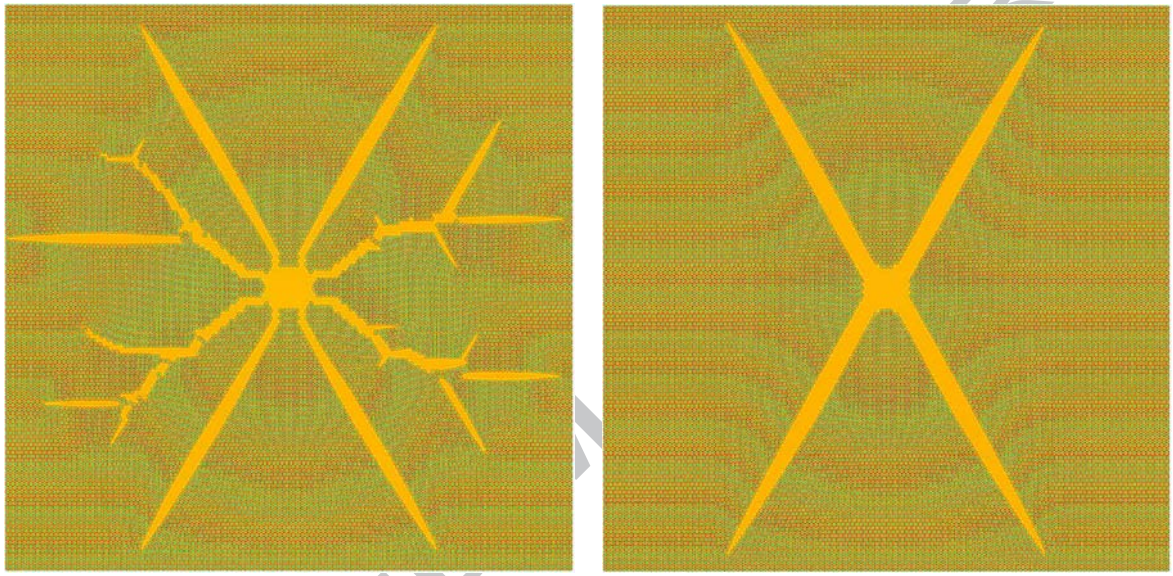

(a) Circular notch. Density at $t = 16000$ (b) Square notch. Density at $t = 15000$

Fig. 3. Crack propagation in a ductile material. The computational domain is $\overline{\Omega} = [0, 1024\pi/3]^2$, and the spatial mesh is composed of 1024^2 $\mathcal{C}^1$ quadratic elements. The time step is $\Delta t = 20$. The initial condition is a crystal lattice with stretchings of approximately 16% and 15% in the x and y directions, respectively. In the center of the domain, we set a small notch. On the left hand side we show the numerical solution using a circular notch of radius $20\pi/3$. For the computation on the right hand side we employed a square notch of side $20\pi/3$.

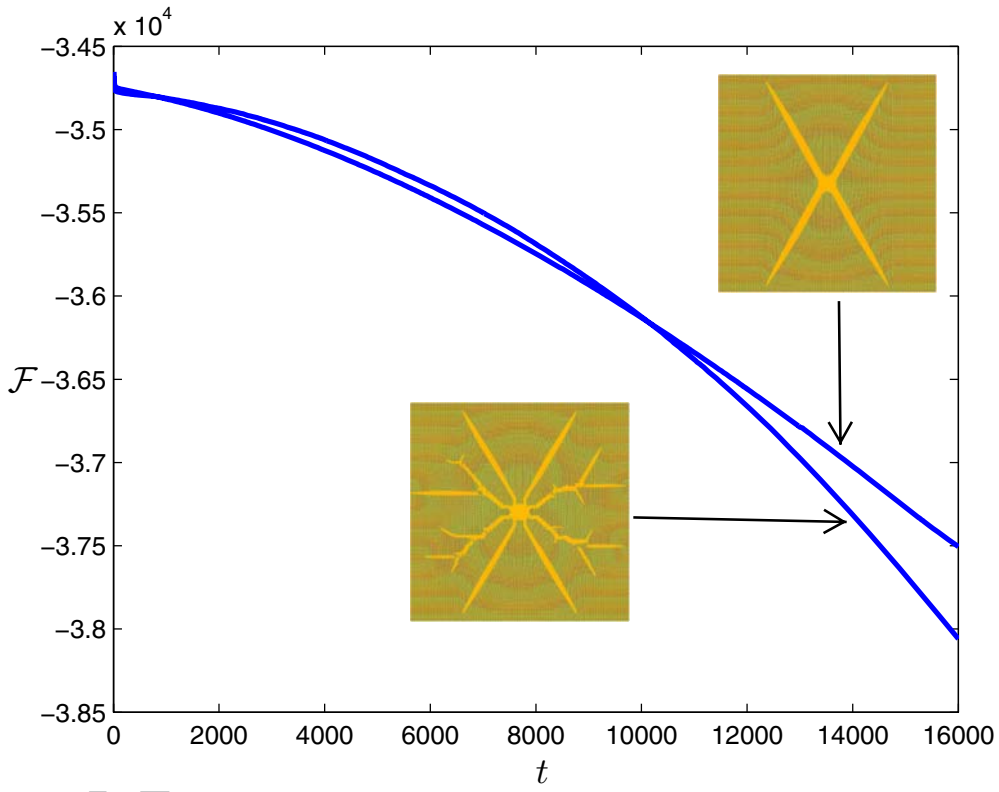

Fig. 4. Crack propagation on a square domain. Time evolution of the energy functional for the two computations presented in Figure 3. We observe that the energy is decreasing at all times.

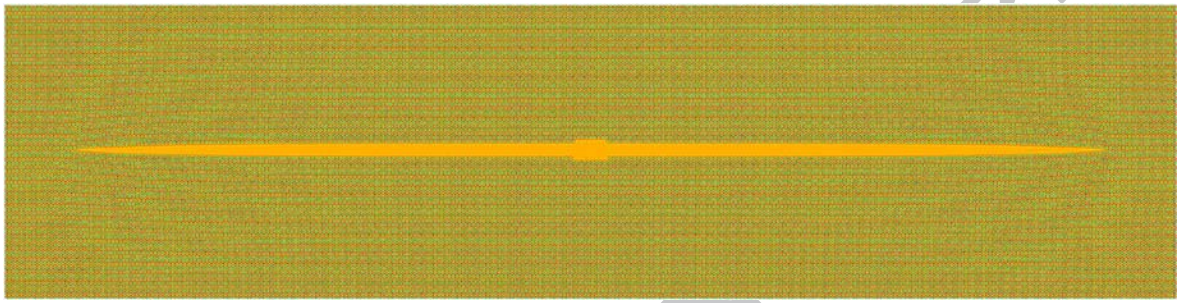

(a) $t = 0$

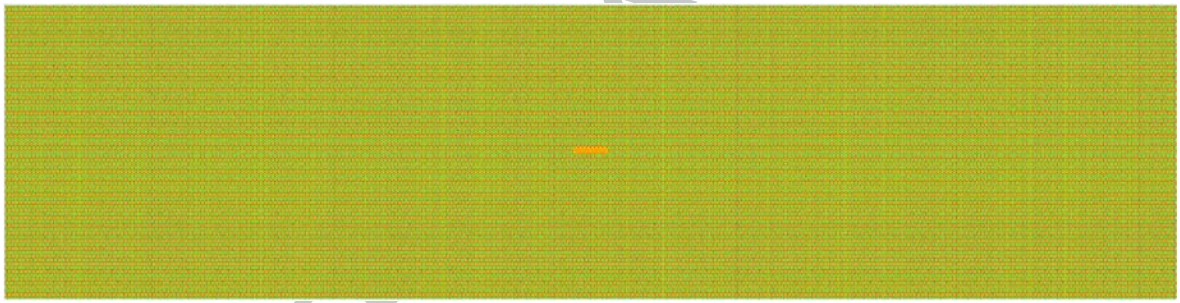

(b) $t = 110000$

Fig. 5. Crack propagation on a rectangular domain. The computational domain is $\overline{\Omega} = [0, 2048\pi/3] \times [0, 512\pi/3]$, and the spatial mesh is composed of 2048×512 $\mathcal{C}^1$ quadratic elements. The time step is $\Delta t = 20$. The initial condition, shown on top, corresponds to Configuration 1. At the bottom we present the numerical solution at time $t = 110000$.

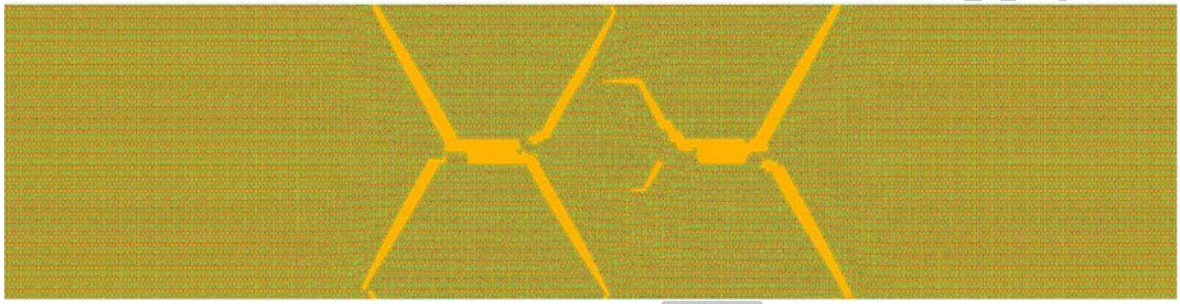

(a) $t = 0$

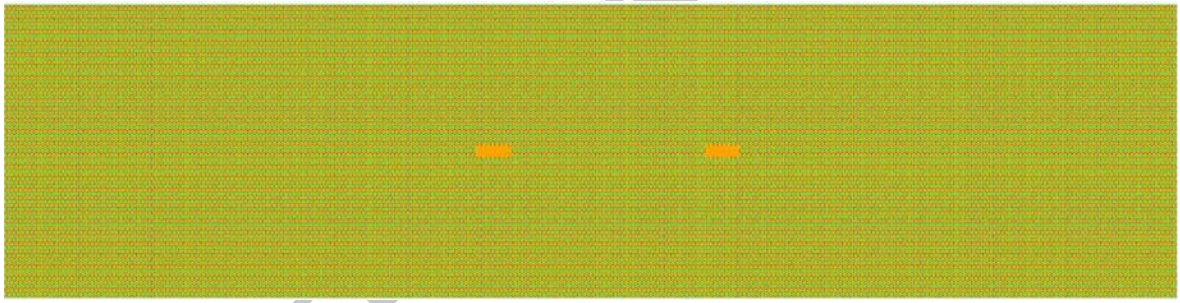

(b) $t = 24000$

Fig. 6. Crack propagation on a rectangular domain. The computational domain is $\overline{\Omega} = [0, 2048\pi/3] \times [0, 512\pi/3]$, and the spatial mesh is composed of 2048×512 $\mathcal{C}^1$ quadratic elements. The time step is $\Delta t = 20$. The initial condition, shown on top, corresponds to Configuration 2. At the bottom we present the numerical solution at time $t = 24000$.

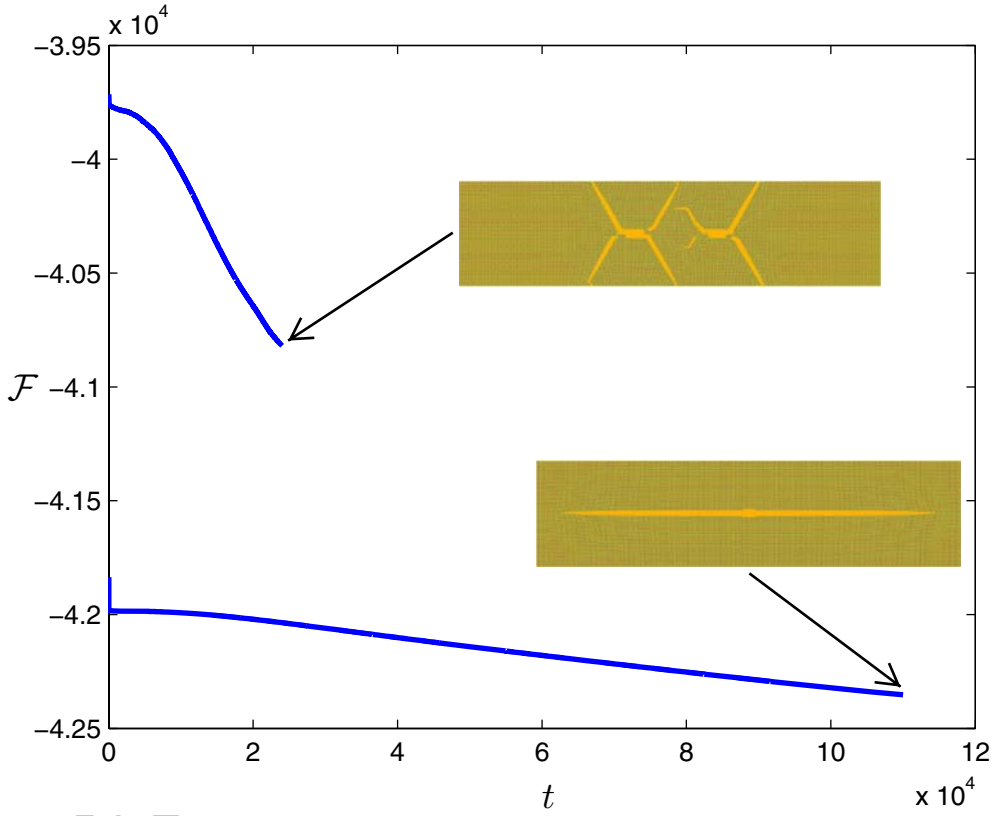

Fig. 7. Crack propagation on a rectangular domain. Time evolution of the free energy for two mechanical configurations. We observe that the free energy is decreasing at all times.

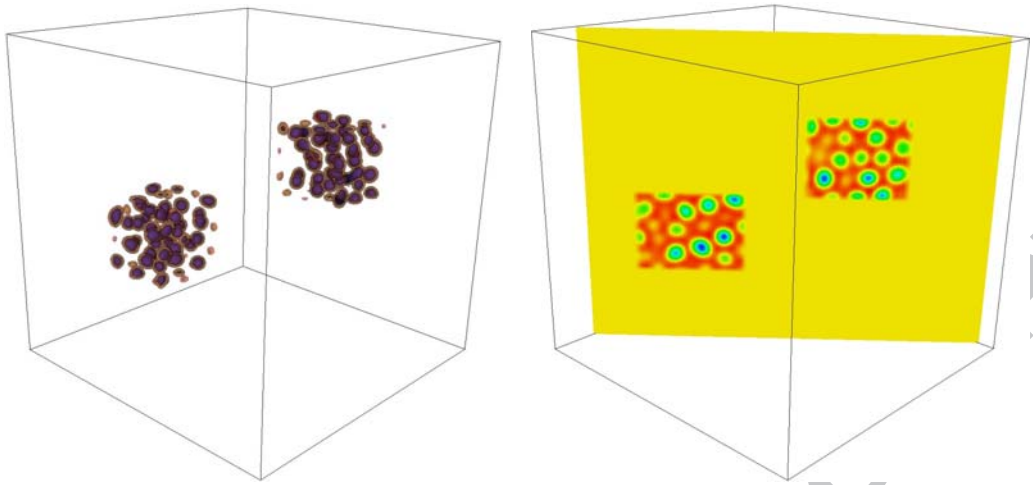

(a) $t = 0$ (b) $t = 0$

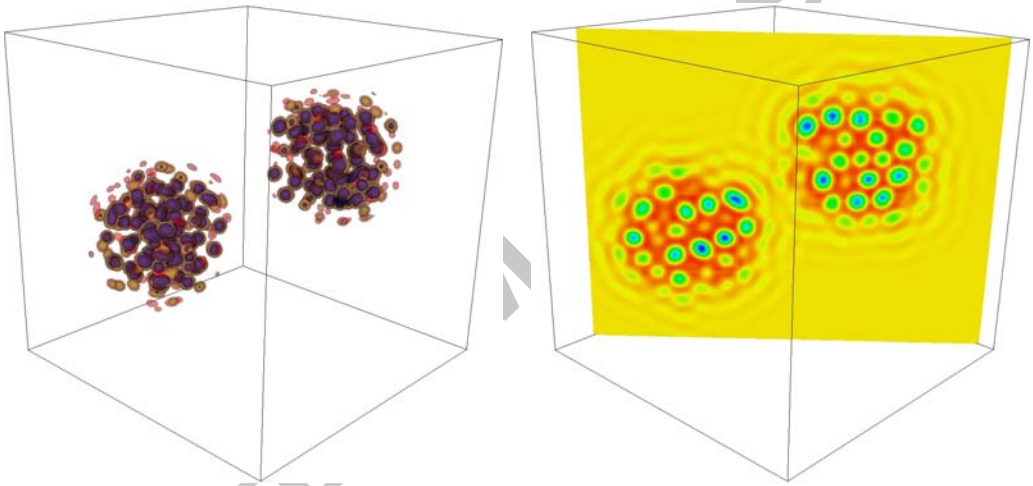

(c) $t = 10$ (d) $t = 10$

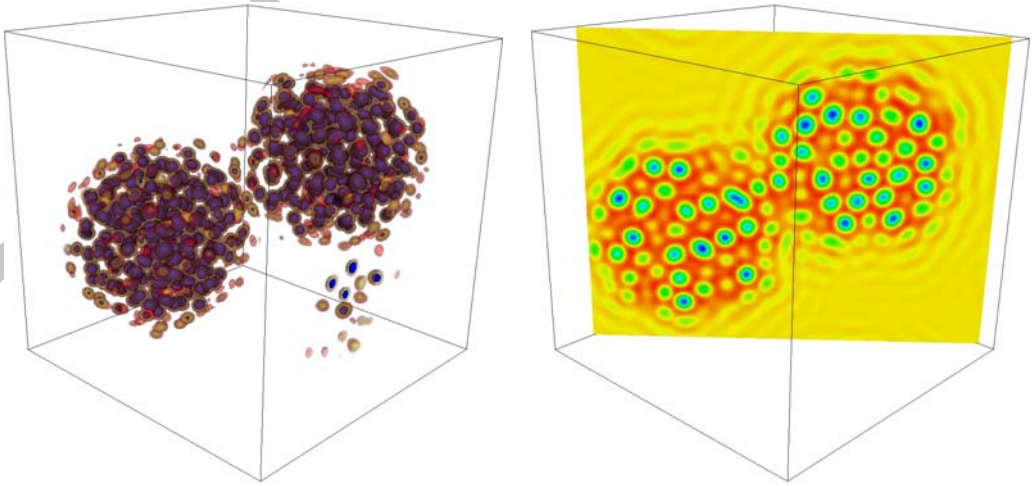

(e) $t = 20$ (f) $t = 20$

Fig. 8. Crystal growth in a supercooled liquid in three dimensions. The images show the evolution and interaction of two crystallites initially surrounded by liquid. The computational times are indicated in the labels. On the left hand side, we show isosurfaces of the solution, while on the right hand side we present a slice of the solution across the indicated plane. The computational mesh is composed of 128^3 $\mathcal{C}^1$ quadratic elements. The time step is $\Delta t = 1$.

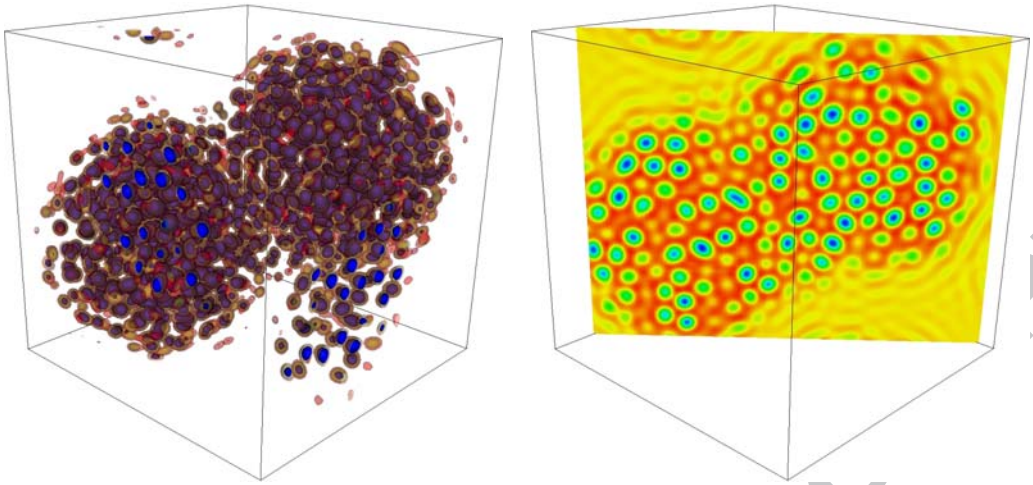

(a) $t = 30$ (b) $t = 30$

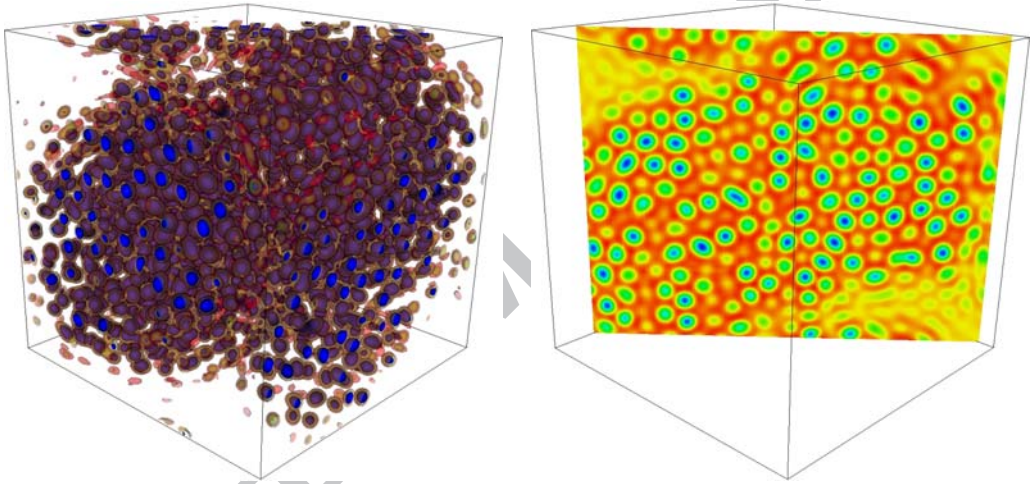

(c) $t = 40$ (d) $t = 40$

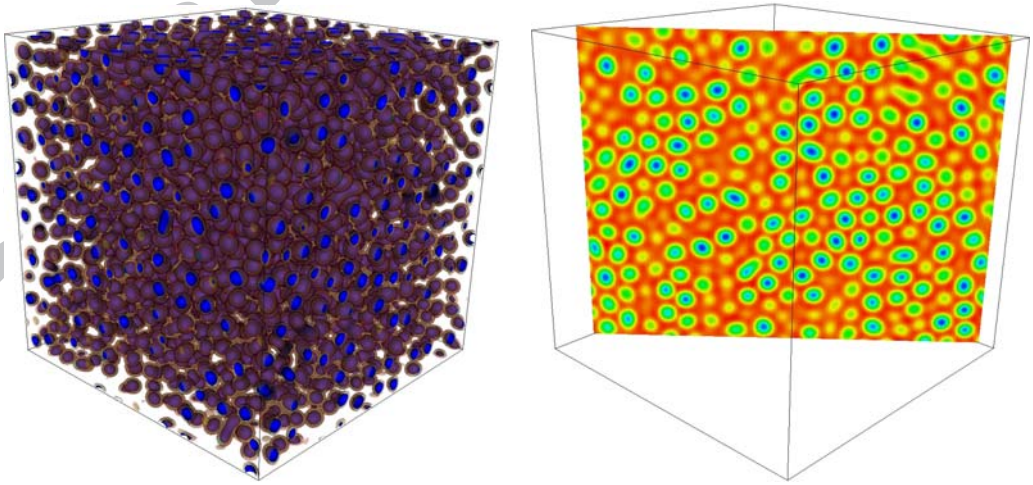

(e) $t = 190$ (f) $t = 190$

Fig. 9. Crystal growth in a supercooled liquid in three dimensions. The images show the evolution and interaction of two crystallites initially surrounded by liquid. The computational times are indicated in the labels. On the left hand side, we show isosurfaces of the solution, while on the right hand side we present a slice of the solution across the indicated plane. The computational mesh is composed of 128^3 $\mathcal{C}^1$ quadratic elements. The time step is $\Delta t = 1$.

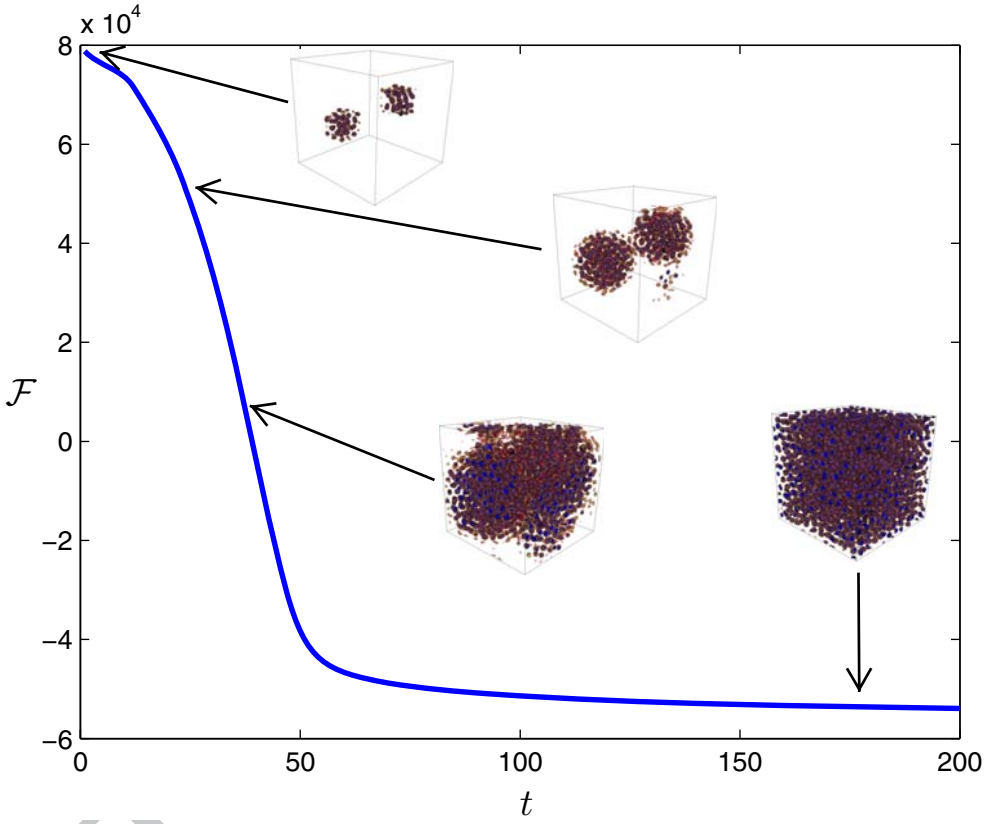

Fig. 10. Crystal growth in a supercooled liquid in three dimensions. The plot shows that the energy is decreasing at all times. We have appended to the energy curve some snapshots of the solution to give an indication of the dynamical process that correspond to the energy decay.

- We propose a new space-time discretization algorithm for the phase field crystal equation.

- The proposed method inherits the nonlinear stability property of the continuum theory.

- We present several numerical examples that support our theoretical results and illustrate the efficiency, accuracy and stability of our new method.